



RS-WorldModel: a Unified Model for Remote Sensing Understanding and Future Sense Forecasting

Linrui Xu^{1*}, Zhongan Wang^{2*}, Fei Shen³, Gang Xu⁴, Huiping Zhuang⁵,
Ming Li^{4†}, and Haifeng Li^{1†}

¹Central South University, ²Zhejiang University, ³National University of Singapore
⁴Guangming Laboratory, ⁵South China University of Technology

Abstract. Remote sensing world models aim to both explain observed changes and forecast plausible futures, two tasks that share spatiotemporal priors. Existing methods, however, typically address them separately, limiting cross-task transfer. We present RS-WorldModel, a unified world model for remote sensing that jointly handles spatiotemporal change understanding and text-guided future scene forecasting, and we build RSWBench-1.1M, a **1.1 million** sample dataset with rich language annotations covering both tasks. RS-WorldModel is trained in three stages: (1) Geo-Aware Generative Pre-training (GAGP) conditions forecasting on geographic and acquisition metadata; (2) synergistic instruction tuning (SIT) jointly trains understanding and forecasting; (3) verifiable reinforcement optimization (VRO) refines outputs with verifiable, task-specific rewards. With only 2B parameters, RS-WorldModel surpasses open-source models up to 120× larger on most spatiotemporal change question-answering metrics. It achieves an FID of 43.13 on text-guided future scene forecasting, outperforming all open-source baselines as well as the closed-source Gemini-2.5-Flash Image (Nano Banana)¹.

Keywords: Cross-modal understanding and generation · World Model · Remote Sensing

1 Introduction

World models, which construct internal representations of environments and predict their future dynamics, have become an active research direction in application domains such as autonomous driving, robotics, and generative simulation [17]. In autonomous driving, GAIA-1 [20] and Drive-WM [47] forecast driving scenes conditioned on planned actions and map context. Video generation systems such as Sora [7] demonstrate that large-scale generative models can serve as

* Equal contribution.

† Corresponding author. (ming.li@u.nus.edu, lihaifeng@csu.edu.cn)

¹ Codes and datasets are available at <https://github.com/GeoX-Lab/RS-WorldModel>

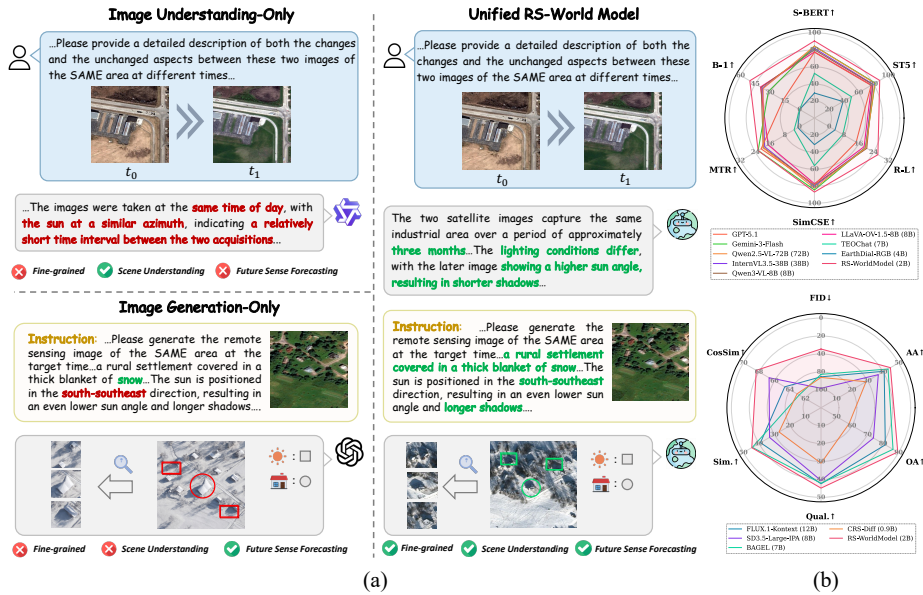


Fig. 1: RS-WorldModel: A unified world model for remote sensing that integrates spatiotemporal change understanding and future scene forecasting capabilities. (a) Qualitative comparison with leading methods. (b) Quantitative results on the RSWBench-1.1M.

versatile physical simulators. In embodied AI, DayDreamer [52] trains robot locomotion and manipulation policies primarily within a learned world model, while Cosmos [1] proposes a general-purpose world foundation model trained on massive video data. These efforts converge on a shared insight: learning to predict future states encourages a model to internalize environment dynamics, making world models a promising path toward general purpose autonomous agents. Earth observation, where satellites repeatedly image the same locations over time, stands to benefit substantially, yet remains unexplored (Figure 1).

Recent remote sensing generative models [62,23] can synthesize plausible satellite imagery, but they are typically confined to pixel-level synthesis without reasoning about *what* changed or *why*. Conversely, understanding-oriented models [26,21,60] interpret observed scenes but are not designed for future or counterfactual states. In many remote sensing settings, applications need *both* accurate interpretation and controllable forecasting [6,44,33]. Both tasks depend on shared priors from geographic and acquisition context (e.g., location, seasonality, and sensor characteristics). Training them separately fails to exploit this shared structure, leaving generation difficult to control and understanding unable to leverage dense generative supervision [59,24].

Building a unified remote sensing world model poses three core challenges. *First*, to the best of our knowledge, no existing dataset simultaneously sup-

ports spatiotemporal change understanding and future scene forecasting at scale; most benchmarks [10,38,11] target a single task and lack the rich geographic metadata needed for location-aware modeling. *Second*, remote sensing imagery exhibits complex spatiotemporal variations driven by geographic location, sensor parameters, and seasonal cycles, making it difficult to learn effective generation priors from limited data [56,45,13]. Existing approaches train understanding and generation in isolation [64,34], limiting knowledge transfer between the two. *Third*, standard reinforcement learning from human feedback relies on learned preference models that fail to capture the geographic consistency and physical plausibility constraints specific to remote sensing [24].

We address these challenges with RS-WorldModel and RSWBench-1.1M. For data, we construct RSWBench-1.1M, a large-scale dataset of **1.1M** high-resolution samples covering both spatiotemporal change understanding and text-guided future scene forecasting, enriched with fine-grained geographic metadata and built on fMoW [11] to ensure global diversity. For modeling, we propose RS-WorldModel, the first unified world model for remote sensing, trained in three stages: (1) Geo-Aware Generative Pre-training (GAGP) injects geographic conditioning to establish spatiotemporal forecasting priors; (2) synergistic instruction tuning (SIT) jointly optimizes understanding and generation to improve controllability and let each task reinforce the other; and (3) verifiable reinforcement optimization (VRO) improves robustness by refining outputs with task-specific verifiable rewards instead of a learned preference model. With only **2B** parameters, RS-WorldModel surpasses open-source models up to $120\times$ larger on most spatiotemporal change QA metrics and achieves an FID of **43.13** on text-guided future scene forecasting, outperforming all open-source baselines and the closed-source Gemini-2.5-Flash Image on FID. Our contributions are as follows:

- We propose RS-WorldModel, the first unified world model for remote sensing that jointly handles spatiotemporal change understanding and text-guided future scene forecasting.
- We construct RSWBench-1.1M, a large-scale dataset of 1.1M samples covering both tasks with rich geographic metadata and fine-grained language annotations.
- We design a three-stage training paradigm (GAGP, SIT, and VRO) that enables a 2B parameter model to outperform far larger open-source models and several closed-source models.

2 RSWBench-1.1M Dataset

Training a unified remote sensing world model requires data supporting two core capabilities: *Spatiotemporal Change Question-Answering* (ST-CQA) and *Text-Guided Future Scene Forecasting* (TFSF). We contribute a scalable automated annotation pipeline and a dataset suite with a 1.1M training corpus and a 5.6K evaluation benchmark. Both are derived from the fMoW archive, with strict adherence to official split protocols to prevent data leakage (Figure 2).

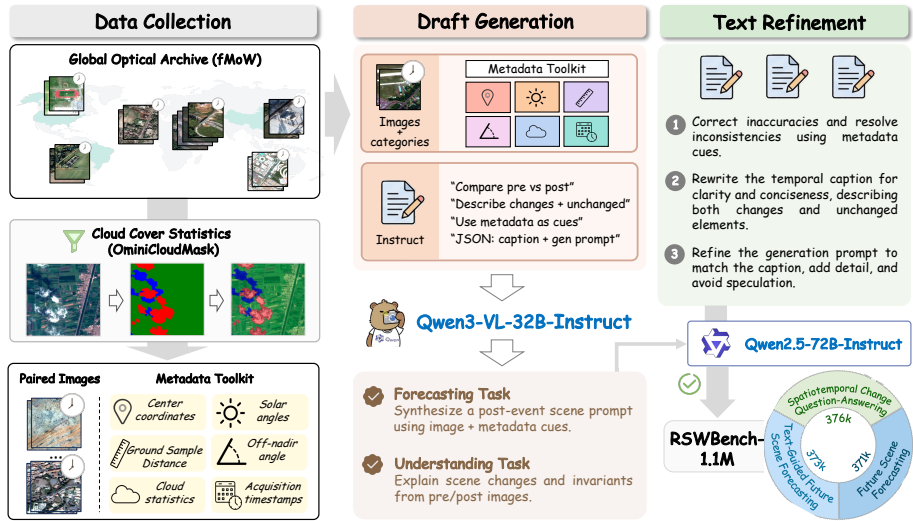


Fig. 2: **Data construction pipeline and dataset composition.** We establish a scalable pipeline to transform multi-temporal observations into high-quality instruction data, supporting understanding and forecasting tasks with strict train-test isolation.

2.1 Scalable Data Construction Pipeline

Constructing a million-scale dataset with spatiotemporal consistency requires overcoming two challenges: atmospheric noise and the lack of dense semantic annotations. We address these via a two-stage pipeline that unifies physical filtering with semantic refinement.

Stage 1: Physical Standardization. We first pair multi-temporal observations from the same geographic coordinates. To ensure the model learns from valid ground features rather than artifacts, we normalize acquisition metadata (e.g., sun angles) and filter samples based on visibility. Using OmniCloudMask [50], we estimate the pixel-wise cloud ratio $\rho_{\text{Cloud}}(I)$ and retain only samples where $\rho_{\text{Cloud}}(I) \leq 0.9$, discarding only near-total occlusions. Unlike conventional remote sensing datasets that enforce strict clear-sky filters (e.g. $\leq 5\text{--}10\%$) [2], we deliberately retain partially cloudy scenes because cloud cover serves as a controllable condition for text-guided Forecasting.

Stage 2: Semantic Refinement. To synthesize high-quality language supervision without expensive manual annotation, we employ a generate-and-refine strategy. A vision-language model first drafts structured JSON annotations based on image pairs and metadata. Subsequently, a larger, more capable model (Qwen2.5-72B-Instruct) refines these drafts. A key design choice is metadata translation: the pipeline explicitly converts raw numeric sensor data into natural linguistic cues (e.g., translating solar elevation into shadow descriptions), preventing the model from overfitting to numerical values.

Table 1: Comparison of dataset capabilities and scales for remote sensing understanding and generation. ✓: supported; ✗: not supported; -: not applicable (dataset does not target this task category).

Dataset	Scale	Understanding		Generation		
		Temporal	Earth Observation	Spatiotemporal Metadata	Observation Environment	Fine-grained Text
EarthDial-Dataset [40]	11.1M	✓	✓	-	-	-
TEOChatlas [22]	554K	✓	✓	-	-	-
FIT-RS [32]	1.8M	✗	✓	-	-	-
MMRS-1M [61]	1.0M	✗	✓	-	-	-
Git-10M [30]	10M	-	-	✗	✓	✗
Street2Sat-Text [58]	72K	-	-	✗	✓	✓
CVACT-Text [58]	88K	-	-	✗	✓	✓
RSWBench-1.1M	1.1M	✓	✓	✓	✓	✓

2.2 RSWBench-1.1M Dataset Suite

Using the pipeline described above, we curate two distinct subsets to support the training and evaluation of remote sensing world models (Table 1).

Training. Constructed exclusively from the fMoW training split, this corpus contains approximately 1.1M samples. It includes 371K instances for generative pre-training and 742K mixed instances for synergistic instruction tuning. An additional 16K subset is reserved for reinforcement alignment.

Evaluation. To establish a rigorous standard, we curate 6.6K samples exclusively from the fMoW test split. The benchmark is balanced, containing 5K ST-CQA and 1.6K TFSSF samples. By preserving the global diversity of the original test set, RSWBench-1.1M enables stable evaluation of cross-region generalization and forecasting fidelity.

3 Method

3.1 Preliminary

Problem Definition. Let I denote a remote sensing image and m its associated geospatial metadata (e.g., coordinates, ground sampling distance, timestamp, sun angles, and cloud statistics). We formulate both *Spatiotemporal Change Question-Answering* (ST-CQA) and *Text-Guided Future Scene Forecasting* (TFSSF) as instruction-conditioned sequence generation tasks. Given a prompt P containing image placeholders $\langle \text{image} \rangle$ and the corresponding metadata m , the objective is to model the conditional probability of the output sequence y :

$$p_{\theta}(y \mid P, I, m). \quad (1)$$

For ST-CQA, y consists of natural language tokens; for TFSSF, y consists of discrete visual tokens.

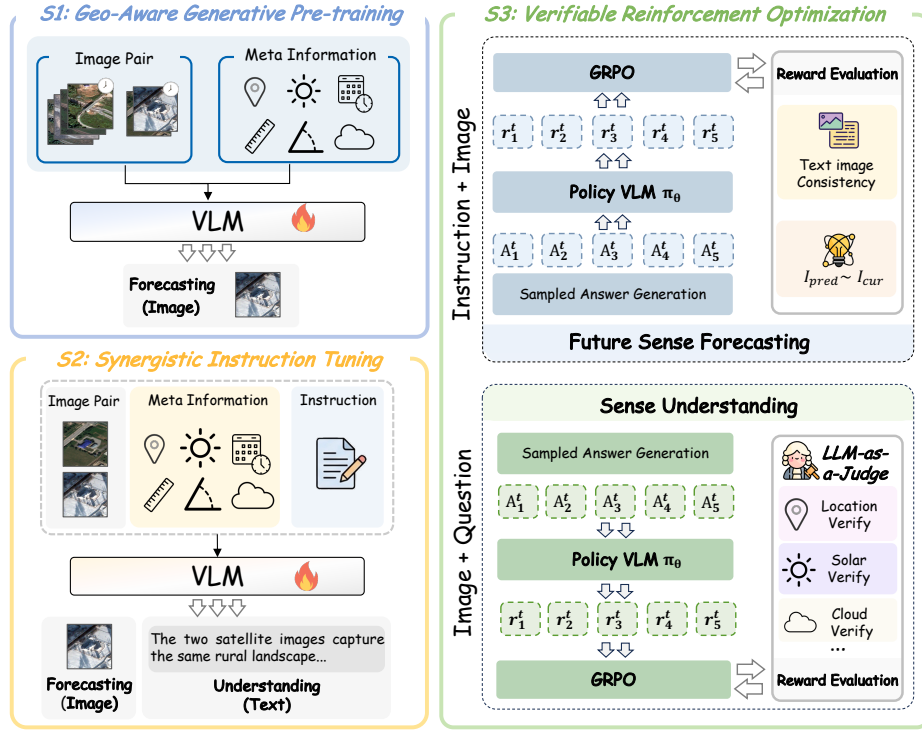


Fig. 3: **Overview of RS-WorldModel.** The framework is a vision-language world model trained via a three-stage pipeline: **S1**: geo-aware generative pre-training on metadata-conditioned image forecasting, **S2**: synergistic instruction tuning for joint understanding and forecasting, and **S3**: verifiable reinforcement optimization with task-specific rewards.

Unified Tokenization and Objective. We employ a MoVQGAN [63] tokenizer (codebook size $K = 16,384$, sequence length $L = 1,024$) to convert each image I (256×256) into discrete visual tokens $z = \text{Tok}(I)$. Both text and visual token generation are treated as a single autoregressive task. The model is trained with next-token prediction on the mixed-modality sequence s :

$$\mathcal{L}_{\text{AR}}(\theta) = - \sum_{i=1}^T \log p_{\theta}(s_i | s_{<i}, P, m), \quad (2)$$

where s_i is either a text or visual token. At inference, visual tokens are decoded as $\hat{I} = \text{Dec}(z)$.

Task-Specific Prompts. The model receives textual prompts that combine visual observations, geospatial metadata, and task-specific language.

For Text-Guided Future Scene Forecasting (TFSF), the prompt includes the current observation (I_{cur}, m_t) , a natural-language instruction T_{ins} describing the

desired changes, and target metadata $m_{t'}$:

$$P_{\text{TFSF}} = \{\mathcal{I}_{\text{cur}}, T_{\text{ins}}, m_t, m_{t'}\}. \quad (3)$$

For geo-aware generative pre-training, we use a simplified text-free version:

$$P_{\text{FSF}} = \{\mathcal{I}_{\text{cur}}, m_t, m_{t'}\}. \quad (4)$$

For Spatiotemporal Change Question-Answering (ST-CQA), the prompt consists of a natural-language question Q about spatiotemporal changes, the bi-temporal pair $(I_{\text{pre}}, I_{\text{post}})$, and the corresponding metadata:

$$P_{\text{ST-CQA}} = \{\mathcal{I}_{\text{pre}}, \mathcal{I}_{\text{post}}, Q, m_{\text{pre}}, m_{\text{post}}\}. \quad (5)$$

Conditioning on both metadata and task-specific text enables the model to separate physical land-cover changes from sensor-induced variations while following user intent.

3.2 RS-WorldModel: A Unified World Model for Remote Sensing

RS-WorldModel is a unified world model designed to perceive, understand, and forecast the spatiotemporal dynamics of Earth’s surface from satellite imagery. Unlike conventional vision-language models trained primarily on natural scenes, RS-WorldModel explicitly encodes the physical rules that govern remote sensing observations—including sun angles, atmospheric conditions, land-cover evolution, and acquisition-time variations within a single autoregressive framework.

Built upon Qwen3-VL-2B-Instruct with only 2B parameters, RS-WorldModel encodes satellite images into visual tokens, fuses them with geospatial metadata, and autoregressively produces mixed-modality outputs: natural-language responses for ST-CQA or discrete visual tokens for future scene forecasting. By treating understanding and forecasting as instances of the same next-token prediction objective in a shared latent space, RS-WorldModel establishes a bidirectional connection between perception and simulation. This unified formulation bridges perception and simulation to advance remote sensing intelligence.

3.3 Learning Remote Sensing World Dynamics

To instill robust physical and semantic priors, RS-WorldModel is trained through three complementary objectives: (1) Geo-Aware Generative Pre-training (GAGP) conditions forecasting on geographic and acquisition metadata; (2) synergistic instruction tuning (SIT) jointly trains understanding and forecasting; and (3) verifiable reinforcement optimization (VRO) that refines outputs with verifiable, task-specific rewards. These objectives progressively build world-modeling capabilities from low-level physical simulation to high-level task alignment (Figure 3). **Geo-Aware Generative Pre-training (GAGP)** performs purely generative pre-training on multi-temporal image sequences without any textual descriptions

or language supervision. For each geographic location, we sample a source observation (I_{cur}, m_t) and a corresponding target observation $(I_{t'}, m_{t'})$. The model is conditioned exclusively on geospatial metadata using the text-free forecasting prompt P_{FSF} to autoregressively predict the target visual token sequence $z_{t'} = \text{Tok}(I_{t'})$:

$$\mathcal{L}_{\text{GAGP}}(\theta) = -\mathbb{E} \left[\sum_{i=1}^{|z_{t'}|} \log p_{\theta}(z_{t',i} \mid z_{t',<i}, P_{\text{FSF}}) \right]. \quad (6)$$

This objective enables the model to condition future scene forecasting directly on geographic and acquisition metadata.

Synergistic instruction tuning (SIT) performs joint instruction tuning on a mixed dataset $\mathcal{D}^{\text{SIT}} = \mathcal{D}_{\text{ST-CQA}} \cup \mathcal{D}_{\text{TFSF}}$. Regardless of output modality (text or visual tokens), the unified next-token prediction objective is optimized:

$$\mathcal{L}_{\text{SIT}}(\theta) = -\mathbb{E}_{(P,y) \sim \mathcal{D}^{\text{SIT}}} \left[\sum_{i=1}^{|y|} \log p_{\theta}(y_i \mid y_{<i}, P) \right]. \quad (7)$$

Prompts are carefully enriched: TFSF prompts incorporate textual constraints to guide specific land-cover transitions, while ST-CQA prompts demand detailed descriptions of both changed and unchanged elements together with explicit reasoning about sensor-induced variations. This synergistic training creates a closed feedback loop that simultaneously improves forecasting controllability and semantic fidelity in understanding.

Verifiable reinforcement optimization (VRO) refines the SIT policy using Group Relative Policy Optimization (GRPO) [19,39] without requiring a separate value network. The optimization operates on both tasks and employs task-specific rewards derived directly from reference signals and prompt metadata—via cosine similarity for TFSF and an LLM judge for ST-CQA—rather than learned reward models, thereby minimizing reward hacking and ensuring reliable alignment.

For the Text-Guided Future Scene Forecasting (TFSF) task, the model outputs a predicted visual-token sequence $z_{\text{pred}} \in \{1, \dots, K\}^L$. These tokens are decoded into pixel space via the frozen decoder to produce the synthesized future image $\hat{I} = \text{Dec}(z_{\text{pred}})$. The conditioning prompt supplies the current image I_{cur} together with the textual instruction T_{ins} . We compute the similarities using a frozen vision-language embedding model $f(\cdot)$ [28]:

$$s_{\text{it}} = \cos\left(f(\hat{I}), f(T_{\text{ins}})\right), \quad s_{\text{ir}} = \cos\left(f(\hat{I}), f(I_{\text{cur}})\right). \quad (8)$$

The final TFSF reward is defined as

$$r_{\text{TFSF}} = s_{\text{it}} + \lambda s_{\text{ir}}, \quad (9)$$

where λ balances description faithfulness against spatial consistency with the current image. This formulation acknowledges the non-unique nature of future

forecasting by rewarding any plausible, condition-consistent outcome rather than enforcing pixel-level matching to a single ground-truth future scene.

For the Spatiotemporal Change Question-Answering (ST-CQA) task, we evaluate the generated caption \hat{y} against the ground-truth reference caption y using an LLM-based judge (Qwen3-30B-A3B-Instruct-2507) [57]. The judge receives the full prompt context together with explicitly parsed spatiotemporal and environmental metadata extracted from the input (coordinates, timestamp, viewing geometry, sun angles, cloud cover statistics, etc.). This metadata grounding enables the judge to detect and penalize contradictions with acquisition conditions (e.g., impossible illumination changes) that traditional n-gram metrics would miss. The LLM outputs a scalar quality score in $[0, 100]$, which is clipped and normalized to produce the final reward:

$$r_{\text{ST-CQA}} = \text{clip}\left(\frac{\text{score}(\hat{y}, y; x)}{100}, 0, 1\right). \quad (10)$$

Compared with BLEU/ROUGE-style overlap metrics, this LLM judge provides semantically richer evaluation of temporal reasoning, change description completeness, and physical plausibility.

The GRPO objective then directly optimizes the policy π_θ by maximizing the group-relative advantage A_{grp} computed over sampled completions while applying KL regularization toward the SIT policy:

$$\max_{\theta} \mathbb{E}[A_{\text{grp}}(x, \hat{y})] - \gamma \text{KL}(\pi_\theta(\cdot | x) \| \pi_{\theta_0}(\cdot | x)). \quad (11)$$

Collectively, GAGP, SIT, and VRO equip RS-WorldModel with a coherent internal world representation of remote sensing dynamics, enabling robust performance on both perception and forecasting tasks.

4 Experiments

4.1 Experimental Setups

Evaluation Benchmarks. We evaluate RS-WorldModel on two tasks. *Spatiotemporal Change Question-Answering* (ST-CQA) measures how well a model describes observed bi-temporal changes; we report GPT-Score, BLEU-1, METEOR, ROUGE-L, S-BERT, SimCSE, ST5-SCS, and average response length on a 5K subset (Table 2). *Text-Guided Future Scene Forecasting* (TFSF) measures whether a model can synthesize a plausible post-temporal image from a text instruction and geographic context; we report FID, CosSim[28], and four GPT-based scores (Similarity, Quality, OA, AA) on a 1.6K subset (Table 3). **Baselines.** For ST-CQA, we compare with closed-source models (GPT-5.1 [35], Gemini-3-Flash [18]), generic open-source VLMs spanning 2B–235B (Qwen-VL series [4], LLaVA-OV [3], InternVL3.5 [46]), and two domain-specific remote sensing models (EarthDial-RGB [40], TEOChat [22]). For TFSF, baselines include closed-source generators (Gemini-2.5-Flash Image [12], GPT-Image-1.5, GPT-Image-1-mini)

Table 2: **Spatiotemporal change question-answering results on the 5K subset.** The table compares RS-WorldModel with commercial, open-source, and domain-specific baselines. Baseline references are provided in Section 4.1.

Method	Size	GPT-S \uparrow	N-Gram			Contextual Similarity			Len
			B-1 \uparrow	MTR \uparrow	R-L \uparrow	S-BERT \uparrow	SimCSE \uparrow	ST5 \uparrow	
<i>Closed-Source Model</i>									
GPT-5.1 [35]	-	91.17	16.82	20.87	14.59	77.19	78.28	76.70	817
Gemini-3-Flash [18]	-	88.02	31.75	22.49	19.64	84.31	84.27	82.22	350
<i>Open-Source Model</i>									
Qwen3-VL-32B [4]	32B	87.79	33.41	25.25	21.67	87.11	84.95	84.10	385
InternVL3.5-38B [46]	38B	83.44	37.80	18.94	19.72	81.74	79.97	79.30	237
Qwen2.5-VL-72B [5]	72B	86.40	37.06	19.78	19.83	84.30	82.11	81.68	310
Qwen3-VL-235B-A22B [4]	235B	87.64	31.25	24.35	20.22	83.10	83.48	81.90	406

Qwen3-VL [4]	2B	75.14	36.79	19.01	21.71	79.47	78.10	77.46	257
	4B	80.85	34.26	22.44	21.75	80.76	79.70	78.01	334
	8B	76.79	39.07	19.68	20.35	80.08	78.43	78.78	238

LLaVA-OV-1.5 [3]	4B	65.85	36.70	15.90	18.79	75.52	76.26	75.00	183
	8B	68.96	39.71	17.09	18.89	77.54	76.91	77.14	202

InternVL3.5 [46]	2B	72.41	31.02	16.60	17.13	77.87	75.81	75.56	259
	4B	78.90	34.76	18.57	18.42	79.14	77.43	77.26	255
	8B	77.05	35.26	18.21	18.02	79.19	77.61	77.30	245
	14B	80.67	34.87	19.42	19.18	80.76	79.33	78.67	263

EarthDial-RGB [40]	4B	17.51	0.00	0.97	3.12	29.34	31.15	38.76	10
TEOChat [22]	7B	36.85	0.03	2.99	7.39	52.38	55.85	50.10	24
RS-WorldModel	2B	86.20	50.59	22.50	26.35	90.45	86.75	88.32	207

and open-source models across different generation paradigms: diffusion-based CRS-Diff [42], adapter-based SD3.5-Large-IPA [43] and FLUX.1-Kontext [27], and the unified model BAGEL [16].

Implementation Details. RS-WorldModel builds on Qwen3-VL-2B-Instruct with the vision encoder and multimodal projector frozen throughout all stages. The *GAGP stage* trains on 371K generation samples, the *SIT stage* fine-tunes on 742K generation and understanding samples, and the *VRO stage* applies GRPO on 16K generation and understanding samples with a KL penalty that combines semantic consistency and perceptual quality rewards. All experiments are conducted on 8 NVIDIA A800 (80 GB) GPUs using DeepSpeed ZeRO-3 and Flash Attention 2. Full hyperparameters are provided in the supplementary material.

4.2 Main Results

Quantitative Results. We report results on both tasks below.

(1) Understanding. Table 2 reports ST-CQA results. With only 2B parameters, RS-WorldModel ranks first among all open-source baselines on BLEU-1, ROUGE-L, and all three contextual similarity metrics. The gain over the same-scale Qwen3-VL-2B is substantial: ROUGE-L improves by 21% and S-BERT by 14%. RS-WorldModel also surpasses models 16–120 \times larger on most metrics, e.g.,

Table 3: **Text-guided future scene forecasting results on the 1.6K subset.** Baseline references are provided in Section 4.1.

Method	Size	FID↓	CosSim↑	GPT Scores↑			
				Sim.	Qual.	OA	AA
<i>Closed-Source Model</i>							
Gemini-2.5-Flash Image [12]	-	46.14	69.21	46.63	46.95	93.58	46.79
GPT-Image-1.5 [37]	-	83.51	66.05	46.94	47.06	94.00	47.00
GPT-Image-1-mini [36]	-	92.27	65.95	44.76	45.96	90.72	45.36
<i>Open-Source Model</i>							
CRS-Diff [42]	0.9B	82.76	63.09	27.04	30.97	58.01	29.01
BAGEL [16]	7B	78.47	62.82	44.25	42.13	86.38	43.19
SD3.5-Large-IPA [43]	8B	97.88	66.69	33.15	40.63	73.78	36.89
FLUX.1-Kontext [27]	12B	81.92	64.67	39.00	42.41	81.41	40.70
RS-WorldModel	2B	43.13	68.34	44.59	44.84	89.43	44.71

Qwen3-VL-32B scores 84.10 on ST5-SCS, while RS-WorldModel reaches 88.32. We attribute this to the three-stage training pipeline. Domain-specific pre-training on 371K remote sensing generation samples (GAGP) anchors temporal reasoning in geospatial context, a capability absent from off-the-shelf VLMs regardless of scale. Joint instruction tuning (SIT) then transfers generation-side spatial knowledge to the understanding task, improving caption completeness. The RL stage (VRO) further refines outputs via a judge-based reward that penalizes metadata-inconsistent descriptions.

Two domain-specific baselines, EarthDial-RGB and TEOChat, score below 40 on GPT-Score, indicating that existing remote sensing models are not designed for open-ended temporal captioning. Among closed-source models, GPT-5.1 [35] achieves the highest GPT-Score but produces responses averaging 817 tokens (nearly 4× the length of RS-WorldModel) with lower n-gram and contextual similarity scores, suggesting verbose but less precise descriptions.

(2) Forecasting. Table 3 reports TFSF results. RS-WorldModel ranks first among all open-source models on every metric, reducing FID by 48% relative to CRS-Diff and by 47% relative to FLUX.1-Kontext while attaining the highest CosSim and GPT scores. A comparison across generation paradigms reveals distinct trade-offs. CRS-Diff, a diffusion model conditioned on change instructions, produces perceptually reasonable images but scores lowest on Similarity, suggesting limited adherence to the textual change description. BAGEL, a unified model like ours, scores competitively on Similarity (44.25) but incurs a substantially higher FID (78.47), indicating text-faithful yet perceptually weaker outputs. RS-WorldModel balances both objectives: its autoregressive formulation with VRO-based reward optimization jointly encourages text faithfulness via s_{it} and perceptual realism via s_{ir} . RS-WorldModel even surpasses the closed-source Gemini-2.5-Flash Image on FID (43.13 vs. 46.14). GPT-Image-1.5 leads on Simi-

Table 4: **Ablation on the reference-adherence weight λ** . Forecasting on the 1.6K subset; understanding on the 5K subset.

λ	Forecasting (TFSF)						Understanding (ST-CQA)						Len	
	FID↓	CosSim↑	GPT Scores↑				GPT-S↑	N-Gram			Contextual Sim.			
			Sim.	Qual.	OA	AA		B-1↑	MTR↑	R-L↑	S-BERT↑	SimCSE↑		ST5↑
0.0	44.19	67.22	44.40	44.34	88.75	44.37	86.03	49.78	22.62	26.05	90.44	86.32	88.07	211
0.1	43.64	67.24	44.23	44.41	88.63	44.32	86.05	49.61	22.79	26.04	90.44	86.47	88.07	214
0.2	43.13	68.34	44.59	44.84	89.43	44.71	86.20	50.59	22.50	26.35	90.45	86.75	88.32	207

larity and OA but with an FID nearly double that of RS-WorldModel, reflecting higher text adherence at the cost of perceptual fidelity.

Qualitative Results. To qualitatively evaluate RS-WorldModel’s capabilities in both understanding and forecasting, we present representative examples from the two core tasks.

(1) Understanding. In the change-understanding scenario (Figure 4), given a pair of high-resolution satellite images of the same urban area captured approximately three years apart, RS-WorldModel accurately reports the overall layout consistency while identifying subtle surface-texture changes near the fire station and correctly attributing differences in shadow length and orientation to variations in sun elevation and acquisition time. In contrast, several strong baselines either overlook all changes or hallucinate major structural modifications.

(2) Forecasting. In the text-guided forecasting scenario (Figure 5), when conditioned on detailed textual descriptions of recreational and commercial scenes, RS-WorldModel produces photorealistic satellite imagery that faithfully preserves tennis-court layouts, parking configurations, vegetation density, building rooftops, shadow directions, and atmospheric lighting outperforming competing diffusion and autoregressive models in structural fidelity and physical consistency.

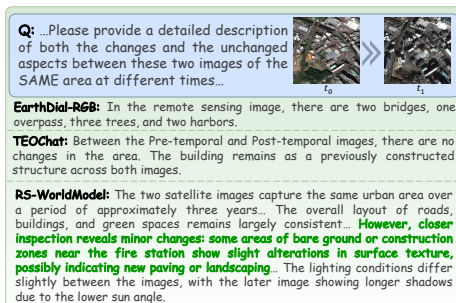


Fig. 4: Qualitative comparison on temporal change understanding.

4.3 Ablation Study

Effect of λ in the TFSF Reward. The hyperparameter λ in Equation (9) balances reference-image consistency (s_{ir}) against text-description faithfulness (s_{it}) in the VRO reward. We sweep $\lambda \in \{0.0, 0.1, 0.2\}$ and report results on both tasks (Table 4). When $\lambda=0$, the reward ignores the reference image entirely, relying on the textual description alone. On TFSF, increasing λ consistently improves all metrics: CosSim rises from 67.22 to 68.34, FID drops from 44.19 to 43.13, and GPT-based OA climbs from 88.75 to 89.43. This confirms that

the reference image supplies valuable spatial priors, including building layouts, road networks, and land-cover distributions that anchor structural plausibility beyond what text alone can convey. On ST-CQA, a consistent trend emerges: GPT-Score improves from 86.03 to 86.20 and BLEU-1 from 49.78 to 50.59 as λ increases, with contextual similarity metrics following the same upward pattern. Only METEOR marginally favors $\lambda=0.1$ (22.79 vs. 22.50). Overall, moderate reference adherence ($\lambda=0.2$) uniformly outperforms both the text-only baseline ($\lambda=0$) and the weaker reference signal ($\lambda=0.1$). We therefore adopt $\lambda=0.2$ for all experiments.



Fig. 5: Qualitative comparison on the text-guided satellite image forecasting task. Given detailed textual prompts, RS-WorldModel generates images with superior structural fidelity, shadow consistency, and scene realism compared to strong baselines.

Table 5: **Ablation on the three-stage training paradigm.** Forecasting on the 1.6K subset; understanding on the 5K subset. *GAGP-only uses metadata conditioning without text instructions.

GAGP	SIT	VRO	Forecasting (TFSF)				ST-CQA		
			FID↓	Sim.↑	Qual.↑	OA↑	AA↑	GPT-S↑	Len
×	✓	×	73.55	39.78	37.64	77.43	38.71	85.63	214
✓	×	×	50.28*	–	–	–	–	–	–
✓	✓	×	44.23	42.38	40.82	83.20	41.56	85.24	201
✓	✓	✓	43.13	44.59	44.84	89.43	44.71	86.20	208

Ablation on Training Stages. We ablate each training stage on the TFSF task (Table 5). Training with SIT alone (no generative pre-training) yields an FID of 73.55, a Similarity score of 39.78, and an OA of 77.43. Adding GAGP before SIT drops FID to 44.23 and raises Similarity to 42.38 and OA to 83.20, showing that generative pre-training on geo-conditioned data provides strong spatial priors for the downstream forecasting task. The VRO stage brings a further improvement: the full three-stage pipeline (GAGP→SIT→VRO) achieves an FID of 43.13, Similarity of 44.59, OA of 89.43, and GPT-S of 86.20, outperforming all partial configurations. GAGP alone already reaches an FID of 50.28, but without SIT the model cannot follow change instructions (GPT scores unavailable). Each stage thus contributes a distinct capability, and removing any one leads to measurable degradation.

Ablation on Geographic Metadata in GAGP. We compare two GAGP variants (Table 6). Without geographic and acquisition metadata conditioning, FID increases from 50.28 to 53.72, confirming that location and sensor information helps the model learn spatially grounded representations during generative pre-training. Qualitatively, we observe that the geo-conditioned model produces land-cover distributions better aligned with the target region, whereas the variant without metadata tends to generate geographically implausible textures. These results suggest that geographic and acquisition metadata serve as an effective spatial prior for the generative pre-training stage.

Table 6: **Geo-metadata ablation in GAGP.** FID on the 1.6K subset.

Pre-training	FID↓
w/o Geo Metadata	53.72
w/ Geo Metadata	50.28

5 Conclusion

We presented RS-WorldModel, a unified world model that jointly addresses spatiotemporal change understanding and text-guided future scene forecasting for remote sensing. Together with RSWBench-1.1M, a 1.1M-sample dataset covering both tasks with fine-grained geographic metadata, RS-WorldModel is trained via a three-stage pipeline: Geo-Aware Generative Pre-training, synergistic instruction

tuning, and verifiable reinforcement optimization. With only 2B parameters, RS-WorldModel surpasses open-source models up to $120\times$ larger on most ST-CQA metrics and outperforms all open-source baselines and the closed-source Gemini-2.5-Flash Image on forecasting FID. Ablations confirm that each training stage contributes a distinct capability and that the verifiable reward design transfers benefits across both tasks.

References

1. Agarwal, N., Ali, A., Bala, M., Balaji, Y., Barker, E., Cai, T., Chattopadhyay, P., Chen, Y., Cui, Y., Ding, Y., et al.: Cosmos world foundation model platform for physical ai. arXiv preprint arXiv:2501.03575 (2025) [2](#)
2. Almar, R., Bergsma, E.W., Thoumyre, G., Giros, A., Marchesiello, P., Lemai-Chenevier, S., Artigues, S., Loyer, S., Delvit, J.M.: Global 1-km coastal bathymetry from sentinel-2 wave inversion using the satellite-to-shores (s2hores) toolbox. *Scientific Data* **12**(1), 1941 (2025) [4](#)
3. An, X., Xie, Y., Yang, K., Zhang, W., Zhao, X., Cheng, Z., Wang, Y., Xu, S., Chen, C., Zhu, D., et al.: Llava-onevision-1.5: Fully open framework for democratized multimodal training. arXiv preprint arXiv:2509.23661 (2025) [9](#), [10](#)
4. Bai, S., Cai, Y., Chen, R., Chen, K., Chen, X., Cheng, Z., Deng, L., Ding, W., Gao, C., Ge, C., Ge, W., Guo, Z., Huang, Q., Huang, J., Huang, F., Hui, B., Jiang, S., Li, Z., Li, M., Li, M., Li, K., Lin, Z., Lin, J., Liu, X., Liu, J., Liu, C., Liu, Y., Liu, D., Liu, S., Lu, D., Luo, R., Lv, C., Men, R., Meng, L., Ren, X., Ren, X., Song, S., Sun, Y., Tang, J., Tu, J., Wan, J., Wang, P., Wang, P., Wang, Q., Wang, Y., Xie, T., Xu, Y., Xu, H., Xu, J., Yang, Z., Yang, M., Yang, J., Yang, A., Yu, B., Zhang, F., Zhang, H., Zhang, X., Zheng, B., Zhong, H., Zhou, J., Zhou, F., Zhou, J., Zhu, Y., Zhu, K.: Qwen3-vl technical report (2025), <https://arxiv.org/abs/2511.21631> [9](#), [10](#)
5. Bai, S., Chen, K., Liu, X., Wang, J., Ge, W., Song, S., Dang, K., Wang, P., Wang, S., Tang, J., et al.: Qwen2. 5-vl technical report. arXiv preprint arXiv:2502.13923 (2025) [10](#)
6. Bastani, F., Wolters, P., Gupta, R., Ferdinando, J., Kembhavi, A.: Satlaspretrain: A large-scale dataset for remote sensing image understanding. In: *Proceedings of the IEEE/CVF International Conference on Computer Vision*. pp. 16772–16782 (2023) [2](#)
7. Brooks, T., Peebles, B., Holmes, C., DePue, W., Guo, Y., Jing, L., Schnurr, D., Taylor, J., Luhman, T., Luhman, E., et al.: Video generation models as world simulators. *OpenAI Blog* **1**(8), 1 (2024) [1](#)
8. Chen, J., Xu, Z., Pan, X., Hu, Y., Qin, C., Goldstein, T., Huang, L., Zhou, T., Xie, S., Savarese, S., et al.: Blip3-o: A family of fully open unified multimodal models-architecture, training and dataset. arXiv preprint arXiv:2505.09568 (2025) [20](#)
9. Chen, X., Wu, Z., Liu, X., Pan, Z., Liu, W., Xie, Z., Yu, X., Ruan, C.: Janus-pro: Unified multimodal understanding and generation with data and model scaling. arXiv preprint arXiv:2501.17811 (2025) [20](#)
10. Chen, Z., Wang, C., Zhang, N., Zhang, F.: Rsccl: A large-scale remote sensing change caption dataset for disaster events. arXiv preprint arXiv:2509.01907 (2025) [3](#)

11. Christie, G., Fendley, N., Wilson, J., Mukherjee, R.: Functional map of the world. In: Proceedings of the IEEE Conference on Computer Vision and Pattern Recognition. pp. 6172–6180 (2018) **3**
12. Comanici, G., Bieber, E., Schaekermann, M., Pasupat, I., Sachdeva, N., Dhillon, I., Blistein, M., Ram, O., Zhang, D., Rosen, E., et al.: Gemini 2.5: Pushing the frontier with advanced reasoning, multimodality, long context, and next generation agentic capabilities. arXiv preprint arXiv:2507.06261 (2025) **9, 11**
13. Cong, Y., Khanna, S., Meng, C., Liu, P., Rozi, E., He, Y., Burke, M., Lobell, D., Ermon, S.: Satmae: Pre-training transformers for temporal and multi-spectral satellite imagery. *Advances in Neural Information Processing Systems* **35**, 197–211 (2022) **3**
14. Cui, Y., Chen, H., Deng, H., Huang, X., Li, X., Liu, J., Liu, Y., Luo, Z., Wang, J., Wang, W., et al.: Emu3. 5: Native multimodal models are world learners. arXiv preprint arXiv:2510.26583 (2025) **20**
15. Dai, M., Liu, S., Zhao, Z., Gao, J., Sun, H., Li, X.: Secure tug-of-war (sectow): Iterative defense-attack training with reinforcement learning for multimodal model security. In: Proceedings of the 33rd ACM International Conference on Multimedia. pp. 11414–11423 (2025) **20**
16. Deng, C., Zhu, D., Li, K., Gou, C., Li, F., Wang, Z., Zhong, S., Yu, W., Nie, X., Song, Z., et al.: Emerging properties in unified multimodal pretraining. arXiv preprint arXiv:2505.14683 (2025) **10, 11**
17. Ding, J., Zhang, Y., Shang, Y., Zhang, Y., Zong, Z., Feng, J., Yuan, Y., Su, H., Li, N., Sukiennik, N., et al.: Understanding world or predicting future? a comprehensive survey of world models. *ACM Computing Surveys* **58**(3), 1–38 (2025) **1**
18. Google: Gemini 3 flash: frontier intelligence built for speed (2025), <https://blog.google/products/gemini/gemini-3-flash/>, published: 2025-12-17; Accessed: 2026-02-26 **9, 10**
19. Guo, D., Yang, D., Zhang, H., Song, J., Wang, P., Zhu, Q., Xu, R., Zhang, R., Ma, S., Bi, X., et al.: Deepseek-r1 incentivizes reasoning in llms through reinforcement learning. *Nature* **645**(8081), 633–638 (2025) **8**
20. Hu, A., Russell, L., Yeo, H., Murez, Z., Fedoseev, G., Kendall, A., Shotton, J., Corrado, G.: Gaia-1: A generative world model for autonomous driving. arXiv preprint arXiv:2309.17080 (2023) **1**
21. Hu, Y., Yuan, J., Wen, C., Lu, X., Liu, Y., Li, X.: Rsgpt: A remote sensing vision language model and benchmark. *ISPRS Journal of Photogrammetry and Remote Sensing* **224**, 272–286 (2025) **2, 20**
22. Irvin, J.A., Liu, E.R., Chen, J.C., Dormoy, I., Kim, J., Khanna, S., Zheng, Z., Ermon, S.: Teoat: A large vision-language assistant for temporal earth observation data. arXiv preprint arXiv:2410.06234 (2024) **5, 9, 10**
23. Khanna, S., Liu, P., Zhou, L., Meng, C., Rombach, R., Burke, M., Lobell, D., Ermon, S.: Diffusionsat: A generative foundation model for satellite imagery. arXiv preprint arXiv:2312.03606 (2023) **2**
24. Köksal, A., Alatan, A.A.: Few-shot vision-language reasoning for satellite imagery via verifiable rewards. In: Proceedings of the IEEE/CVF International Conference on Computer Vision. pp. 6901–6910 (2025) **2, 3**
25. Köksal, A., Alatan, A.A.: Samchat: Introducing chain-of-thought reasoning and grpq to a multimodal small language model for small-scale remote sensing. *IEEE Journal of Selected Topics in Applied Earth Observations and Remote Sensing* **19**, 795–804 (2025) **20**

26. Kuckreja, K., Danish, M.S., Naseer, M., Das, A., Khan, S., Khan, F.S.: Geochat: Grounded large vision-language model for remote sensing. In: Proceedings of the IEEE/CVF Conference on Computer Vision and Pattern Recognition. pp. 27831–27840 (2024) [2](#), [20](#)
27. Labs, B.F., Batifol, S., Blattmann, A., Boesel, F., Consul, S., Diagne, C., Dockhorn, T., English, J., English, Z., Esser, P., et al.: Flux. 1 kontekst: Flow matching for in-context image generation and editing in latent space. arXiv preprint arXiv:2506.15742 (2025) [10](#), [11](#)
28. Li, M., Zhang, Y., Long, D., Chen, K., Song, S., Bai, S., Yang, Z., Xie, P., Yang, A., Liu, D., et al.: Qwen3-vl-embedding and qwen3-vl-reranker: A unified framework for state-of-the-art multimodal retrieval and ranking. arXiv preprint arXiv:2601.04720 (2026) [8](#), [9](#)
29. Li, X., Ding, J., Elhoseiny, M.: Vrsbench: A versatile vision-language benchmark dataset for remote sensing image understanding. Advances in Neural Information Processing Systems **37**, 3229–3242 (2024) [20](#)
30. Liu, C., Chen, K., Zhao, R., Zou, Z., Shi, Z.: Text2earth: Unlocking text-driven remote sensing image generation with a global-scale dataset and a foundation model. IEEE Geoscience and Remote Sensing Magazine (2025) [5](#)
31. Lu, W., Tong, Y., Ye, Z.: Dammfnd: Domain-aware multimodal multi-view fake news detection. In: Proceedings of the AAAI Conference on Artificial Intelligence. vol. 39, pp. 559–567 (2025) [20](#)
32. Luo, J., Pang, Z., Zhang, Y., Wang, T., Wang, L., Dang, B., Lao, J., Wang, J., Chen, J., Tan, Y., et al.: Skysensegpt: A fine-grained instruction tuning dataset and model for remote sensing vision-language understanding. arXiv preprint arXiv:2406.10100 (2024) [5](#), [21](#)
33. Mall, U., Hariharan, B., Bala, K.: Change-aware sampling and contrastive learning for satellite images. In: Proceedings of the IEEE/CVF Conference on Computer Vision and Pattern Recognition. pp. 5261–5270 (2023) [2](#)
34. Muhtar, D., Li, Z., Gu, F., Zhang, X., Xiao, P.: Lhrs-bot: Empowering remote sensing with vgi-enhanced large multimodal language model. In: European Conference on Computer Vision. pp. 440–457. Springer (2024) [3](#)
35. OpenAI: Gpt-5.1: A smarter, more conversational chatgpt (2025), <https://openai.com/index/gpt-5-1/>, published: 2025-11-12; Accessed: 2026-02-26 [9](#), [10](#), [11](#)
36. OpenAI: gpt-image-1-mini model (2025), <https://platform.openai.com/docs/models/gpt-image-1-mini>, accessed: 2026-02-26 [11](#)
37. OpenAI: Gpt image 1.5 model (2025), <https://platform.openai.com/docs/models/gpt-image-1.5>, accessed: 2026-02-26 [11](#)
38. Revankar, S., Mall, U., Phoo, C.P., Bala, K., Hariharan, B.: Monitrs: Multimodal observations of natural incidents through remote sensing. arXiv preprint arXiv:2507.16228 (2025) [3](#)
39. Shao, Z., Wang, P., Zhu, Q., Xu, R., Song, J., Bi, X., Zhang, H., Zhang, M., Li, Y., Wu, Y., et al.: Deepseekmath: Pushing the limits of mathematical reasoning in open language models. arXiv preprint arXiv:2402.03300 (2024) [8](#)
40. Soni, S., Dudhane, A., Debary, H., Fiaz, M., Munir, M.A., Danish, M.S., Fraccaro, P., Watson, C.D., Klein, L.J., Khan, F.S., et al.: Earthdial: Turning multi-sensory earth observations to interactive dialogues. In: Proceedings of the Computer Vision and Pattern Recognition Conference. pp. 14303–14313 (2025) [5](#), [9](#), [10](#)
41. Sun, S., Yu, W., Ren, Y., Du, W., Liu, L., Zhang, X., Hu, Y., Ma, C.: Gdiffretro: Retrosynthesis prediction with dual graph enhanced molecular representation and diffusion generation. In: Proceedings of the AAAI Conference on Artificial Intelligence. vol. 39, pp. 12595–12603 (2025) [20](#)

42. Tang, D., Cao, X., Hou, X., Jiang, Z., Liu, J., Meng, D.: Crs-diff: Controllable remote sensing image generation with diffusion model. *IEEE Transactions on Geoscience and Remote Sensing* (2024) [10](#), [11](#)
43. Team, I.: Instantx sd3.5-large ip-adapter page (2024) [10](#), [11](#)
44. Van Etten, A., Hogan, D., Manso, J.M., Shermeyer, J., Weir, N., Lewis, R.: The multi-temporal urban development spacenet dataset. In: *Proceedings of the IEEE/CVF Conference on Computer Vision and Pattern Recognition*. pp. 6398–6407 (2021) [2](#)
45. Wang, J., Xuan, W., Qi, H., Liu, Z., Liu, K., Wu, Y., Chen, H., Song, J., Xia, J., Zheng, Z., et al.: Disasterm3: A remote sensing vision-language dataset for disaster damage assessment and response. *arXiv preprint arXiv:2505.21089* (2025) [3](#)
46. Wang, W., Gao, Z., Gu, L., Pu, H., Cui, L., Wei, X., Liu, Z., Jing, L., Ye, S., Shao, J., et al.: Internvl3. 5: Advancing open-source multimodal models in versatility, reasoning, and efficiency. *arXiv preprint arXiv:2508.18265* (2025) [9](#), [10](#)
47. Wang, Y., He, J., Fan, L., Li, H., Chen, Y., Zhang, Z.: Driving into the future: Multiview visual forecasting and planning with world model for autonomous driving. In: *Proceedings of the IEEE/CVF Conference on Computer Vision and Pattern Recognition*. pp. 14749–14759 (2024) [1](#)
48. Wang, Z., Prabha, R., Huang, T., Wu, J., Rajagopal, R.: Skyscript: A large and semantically diverse vision-language dataset for remote sensing. In: *Proceedings of the AAAI Conference on Artificial Intelligence*. vol. 38, pp. 5805–5813 (2024) [21](#)
49. Weng, X., Pang, C., Xia, G.S.: Vision-language modeling meets remote sensing: Models, datasets, and perspectives. *IEEE Geoscience and Remote Sensing Magazine* (2025) [20](#)
50. Wright, N., Duncan, J.M., Callow, J.N., Thompson, S.E., George, R.J.: Training sensor-agnostic deep learning models for remote sensing: Achieving state-of-the-art cloud and cloud shadow identification with omnisclocloudmask. *Remote Sensing of Environment* **322**, 114694 (2025) [4](#)
51. Wu, C., Chen, X., Wu, Z., Ma, Y., Liu, X., Pan, Z., Liu, W., Xie, Z., Yu, X., Ruan, C., et al.: Janus: Decoupling visual encoding for unified multimodal understanding and generation. In: *Proceedings of the Computer Vision and Pattern Recognition Conference*. pp. 12966–12977 (2025) [20](#)
52. Wu, P., Escontrela, A., Hafner, D., Abbeel, P., Goldberg, K.: Daydreamer: World models for physical robot learning. In: *Conference on robot learning*. pp. 2226–2240. PMLR (2023) [2](#)
53. Xiao, T., Xu, X., Huang, Z., Gao, H., Liu, Q., Liu, Q., Chen, E.: Perception-r1: Advancing multimodal reasoning capabilities of mllms via visual perception reward. *arXiv preprint arXiv:2506.07218* (2025) [25](#)
54. Xie, J., Yang, Z., Shou, M.Z.: Show-o2: Improved native unified multimodal models. *arXiv preprint arXiv:2506.15564* (2025) [20](#)
55. Xu, L., Zhao, L., Guo, W., Li, Q., Long, K., Zou, K., Wang, Y., Li, H.: Rsgpt4v: A unified multimodal instruction-following dataset for remote sensing image understanding. *arXiv preprint arXiv:2406.12479* (2024) [21](#)
56. Xuan, W., Wang, J., Qi, H., Chen, Z., Zheng, Z., Zhong, Y., Xia, J., Yokoya, N.: Dynamicv1: Benchmarking multimodal large language models for dynamic city understanding. *arXiv preprint arXiv:2505.21076* (2025) [3](#)
57. Yang, A., Li, A., Yang, B., Zhang, B., Hui, B., Zheng, B., Yu, B., Gao, C., Huang, C., Lv, C., et al.: Qwen3 technical report. *arXiv preprint arXiv:2505.09388* (2025) [9](#)
58. Ye, J., He, J., Zhang, X., Lin, Y., Lin, H., He, C., Li, W.: Satellite image synthesis from street view with fine-grained spatial textual guidance: A novel framework. *IEEE Geoscience and Remote Sensing Magazine* (2025) [5](#), [21](#)

59. Zeng, S., Chang, X., Xie, M., Liu, X., Bai, Y., Pan, Z., Xu, M., Wei, X., Guo, N.: Futuresightdrive: Thinking visually with spatio-temporal cot for autonomous driving. arXiv preprint arXiv:2505.17685 (2025) [2](#), [20](#)
60. Zhan, Y., Xiong, Z., Yuan, Y.: Skyeyegpt: Unifying remote sensing vision-language tasks via instruction tuning with large language model. ISPRS Journal of Photogrammetry and Remote Sensing **221**, 64–77 (2025) [2](#), [20](#)
61. Zhang, W., Cai, M., Zhang, T., Zhuang, Y., Mao, X.: Earthgpt: A universal multimodal large language model for multisensor image comprehension in remote sensing domain. IEEE Transactions on Geoscience and Remote Sensing **62**, 1–20 (2024) [5](#), [20](#)
62. Zhao, Z., Wu, C., Cao, X., Wang, D., Chen, H., Tang, D., Zhang, L., Zheng, Z.: Changebridge: Spatiotemporal image generation with multimodal controls for remote sensing. arXiv preprint arXiv:2507.04678 (2025) [2](#)
63. Zheng, C., Vuong, T.L., Cai, J., Phung, D.: Movq: Modulating quantized vectors for high-fidelity image generation. Advances in Neural Information Processing Systems **35**, 23412–23425 (2022) [6](#)
64. Zhu, Q., Lao, J., Ji, D., Luo, J., Wu, K., Zhang, Y., Ru, L., Wang, J., Chen, J., Yang, M., et al.: Skysense-o: Towards open-world remote sensing interpretation with vision-centric visual-language modeling. In: Proceedings of the Computer Vision and Pattern Recognition Conference. pp. 14733–14744 (2025) [3](#), [20](#)

The appendix includes the following sections:

- Appendix A: Related Work
- Appendix B: Details about RSWBench-1.1M Dataset
- Appendix C: Additional Implementation Details
- Appendix D: Case Studies
- Appendix E: Prompts

A Related Work

A.1 Unified multimodal understanding and generation

Recent studies highlight the advantages of unified multimodal models that jointly handle visual understanding and controllable generation within a single autoregressive framework [51,9,8], enabling bidirectional knowledge transfer via shared representations and yielding stronger semantic consistency, generation controllability, and emergent world-modeling capabilities. Methods like Show-o2 [54] represent visual information through discrete tokenization and train large language models to perform autoregressive next-token prediction. However, they often suffer from insufficient semantic preservation and degraded downstream understanding performance. Alternatives using continuous encoders typically rely on external diffusion models or mismatched objectives [14], resulting in complex designs and prohibitive billion-scale pretraining costs. Inspired by FutureSight-Drive [59], we unify spatiotemporal change understanding and text-guided future scene forecasting through a shared tokenizer and a single next-token prediction objective on mixed text-visual sequences, achieving competitive results with only approximately 1% of the training costs of prior methods [51,41,31,15].

A.2 Vision-language models for Remote Sensing

Vision-language models for remote sensing have produced several strong understanding oriented approaches [49]. GeoChat [26] introduces grounded spatial reasoning, while RSGPT [21] establishes a comprehensive benchmark for VQA, captioning, and other understanding tasks. SkyEyeGPT [60] unifies diverse RS tasks via large-scale instruction tuning, and Skysense-o [64] pushes toward open-world interpretation with a vision-centric design. EarthGPT [61] further extends to multisensor comprehension. More recent efforts, such as SAMChat [25], incorporate chain-of-thought reasoning to improve efficiency on small-scale remote sensing images. Nevertheless, these methods focus exclusively on perception and lack native support for controllable future scene generation or unified world modeling.

A.3 Large-Scale Remote Sensing Vision-Language Datasets

Large-scale remote sensing vision-language datasets have been developed to support multimodal understanding tasks. VRSBench [29] serves as a versatile

across tasks, and the rich semantic coverage achieved through our automated annotation pipeline.

C Additional Implementation Details

Training details. RS-WorldModel is built on Qwen3-VL-2B-Instruct. Across all three stages, we freeze the vision encoder and the multimodal projector and train the remaining parameters in bf16 on 8 NVIDIA A800 GPUs (80 GB each), using DeepSpeed ZeRO-3 and Flash Attention 2. For Stages 1 and 2, we cap the image resolution at 524,288 pixels and the video resolution at 16,384 pixels, with a context length of 32,768 tokens and a maximum generation length of 2,048 tokens. We further introduce dedicated tokens for geographic coordinates, ground sampling distance, timestamps, sun angles, off-nadir angle, and cloud cover, allowing acquisition metadata to be serialized together with the visual context.

In Stage 1, we carry out geo-aware generative pre-training on 371K forecasting samples for 32 epochs with a per-device batch size of 16 and gradient accumulation of 2. We use a cosine schedule with a peak learning rate of 5×10^{-4} and a warmup ratio of 0.10. Stage 2 starts from the Stage-1 checkpoint and is trained for another 32 epochs on 742K mixed understanding and forecasting samples. The batch configuration remains unchanged, while the peak learning rate is reduced to 1×10^{-4} and the warmup ratio to 0.02. In both stages, 10% of the training data is held out for validation; the evaluation batch size is 16, and evaluation is performed every 1000 steps.

In Stage 3, we continue from the Stage-2 checkpoint and apply GRPO on 16K mixed ST-CQA and TFSF samples. For TFSF, we use the reward in Eq. (9) with $\lambda = 0.2$, selected by the ablation study in the main paper. For ST-CQA, we adopt Qwen3-30B-A3B-Instruct-2507 as the judge model. We retain KL regularization throughout reinforcement optimization to keep the policy close to the Stage-2 initialization and preserve the instruction-following behavior learned during instruction tuning.

D Case Studies

We present two representative case studies to qualitatively demonstrate RS-WorldModel’s superiority in both core tasks. In the spatiotemporal change understanding task (Figure 8), given a bi-temporal pair with the instruction “Please provide a detailed description of both the changes and the unchanged aspects between these two images of the SAME area at different times”, most baselines either overlook subtle changes or hallucinate major modifications. In contrast, RS-WorldModel accurately identifies layout consistency, vegetation growth, and acquisition-time shadow variations, achieving the highest GPT-Score.

Q: ...Please provide a detailed description of both the changes and the unchanged aspects between these two images of the SAME area at different times...

EarthDial-R6B: There is no change to mention between the two images. **Score:40**

TEOChat: Between the Pre-temporal and Post-temporal images, there have been no changes to the area. The building remains as a previously constructed structure in both images. **Score:45**

LLaVA-OV-1.5-4B: ... The pre-temporal image shows a clear day ... the sun was lower in the sky, casting longer shadows ... The post-temporal image also shows a clear day, but the sun is higher, resulting in shorter shadows ... A large building that was previously empty has now been constructed, and there are new roads and parking lots that were not present before ... The surrounding trees have grown taller ... Overall, the area has undergone significant development and growth since the pre-temporal image was taken. **Score:35**

LLaVA-OV-1.5-8B: ... The buildings within the area have undergone some modifications ... Some structures appear to have been expanded or altered in shape, indicating possible construction or renovation activities ... The layout of the roads seems to have changed slightly, with some sections appearing wider or having additional lanes, which could imply road expansion or traffic management adjustments ... The overall shape and size of the central building complex remain consistent ... The general pattern of the surrounding roads and their connections ... have not changed significantly. **Score:73**

InternVL3.5-4B: ... The arrangement and presence of most buildings remain consistent ... Major roads and open clearings ... maintain their layout ... The large industrial complex at the bottom right ... is unchanged in position and appearance ... The landscaped areas ... are now fully covered with lush green trees ... there has been a noticeable change in vegetation ... The sunlight angle and elevation have changed significantly ... Post-temporal sunlight is higher and more direct compared to the Pre-temporal image. **Score:72**

InternVL3.5-8B: ... The area has seen increased construction and urban sprawl ... New buildings and structures are more visible in the post-temporal image, indicating expansion and development in the urban landscape ... There is noticeable growth in greenery, particularly along roads and in previously open areas ... Roads and pathways may have been widened or altered ... The overall layout of major buildings and infrastructure seems to retain its core structure ... the fundamental structure of the area remains recognizable across the time frames. **Score:75**

Qwen3-VL-4B: ... the most noticeable change is the significant increase in vegetation cover ... in the post-temporal image, dense green foliage has taken over, suggesting seasonal growth or the passage of time ... The road network, including the highway and intersecting streets, remains unchanged in layout and structure ... Buildings and industrial structures ... remain visually identical in shape, size, and placement ... However, this does not affect the underlying features ... the changes observed are purely in the vegetation and seasonal growth patterns, not in the built environment or infrastructure. **Score:80**

Qwen3-VL-8B: ... A new road segment appears in the lower right portion of the second image, connecting to the existing highway ... the layout of roads near the central buildings has been adjusted ... there seems to be an addition or modification to the structure itself, possibly involving a new roof or expansion ... The major highway running horizontally through the center of the scene remains largely unchanged ... The large, prominent building complex located centrally ... retain their fundamental form and location relative to each other. **Score:58**

RS-WorldModel: ... The overall layout of roads, parking lots, and buildings remains consistent ... The central ground transportation station ... retains its position and general footprint ... The surrounding parking areas show minor variations in vehicle density and arrangement, likely due to daily or seasonal fluctuations rather than permanent changes ... Vegetation near buildings appears more lush and mature in the later image ... the later image showing a higher sun angle and shorter shadows. **Score:93**



Fig. 8: **ST-CQA case study.** Model responses with GPT-Scores. RS-WorldModel achieves the best score.

For the text-guided future scene forecasting task (Figure 9), across three diverse scenarios with identical textual instructions and geographic metadata, RS-WorldModel generates images with superior structural fidelity, shadow consistency, and text adherence, consistently attaining the highest GPT-based Similarity and Quality scores among strong open-source baselines.



Fig. 9: **TFSF case study.** Generated results for three textual instructions. RS-WorldModel obtains the highest GPT-based scores.

E Prompts

To ensure reproducibility, we present all prompt templates used in our data construction, evaluation, and training pipeline. These prompts are carefully engineered for their respective roles: the *Qwen3-VL-32B Draft Generation Prompt* (Figure 10) and *Qwen2.5-72B Text Refinement Prompt* (Figure 11) enable scalable, high-quality annotation of RSWBench-1.1M; the *GPT-5-Nano ST-CQA*

Scoring Prompt (Figure 12) and *GPT-4o TFSSF Scoring Prompt* (Figure 15) provide reliable automatic scoring for understanding and generation tasks; the *Qwen3 LLM-as-a-Judge Prompt* (Figure 16) drives verifiable reinforcement optimization (VRO); and the *Stage-1 System Prompt* (Figure 13) together with the *Stage-2/3 System Prompt* (Figure 14) define RS-WorldModel’s behavior across training stages. In particular, we adopt a pure LLM as the judge in VRO, inspired by Perception-R1 [53], rather than a VLM. This design delivers more stable, semantically rich, and metadata-grounded reward signals for geographic and physical plausibility.

Draft Generation Prompt

System Prompt

You are an advanced AI model capable of combining geospatial metadata to generate temporal captions describing both changes and unchanged aspects between two temporal image phases, as well as constructing text prompts for generating post-temporal images.

You will be provided with two satellite images of the same geographic location, centered at coordinates (latitude, longitude) (`{center_lat_lon}`), but captured at different times. Geospatial metadata includes:

- **Acquisition times:** Pre-temporal image at `{time[0]}`, Post-temporal image at `{time[1]}`.
- **Bounding boxes for key objects** (normalized coordinates in the range `[0, 1000]`): Pre-temporal image `{"bbox_2d": {new_xyxy_box[0]}, "label": "{category[0]}"`, Post-temporal image `{"bbox_2d": {new_xyxy_box[1]}, "label": "{category[1]}"`.
- **Sun azimuth:** Pre-temporal image `{sun_azimuth[0]}` degrees, Post-temporal image `{sun_azimuth[1]}` degrees.
- **Sun elevation:** Pre-temporal image `{sun_elevation[0]}` degrees, Post-temporal image `{sun_elevation[1]}` degrees.
- **Off-nadir angle:** Pre-temporal image `{off_nadir_angle[0]}` degrees, Post-temporal image `{off_nadir_angle[1]}` degrees.
- **Cloud cover:** Pre-temporal image `{cloud_cover[0]}`%, Post-temporal image `{cloud_cover[1]}`%.

<metadata-interpretation-guide>

- **Hemisphere:** Positive latitude = Northern; negative = Southern.
- **Seasons (month-based):**
 - Northern: Mar-May (spring), Jun-Aug (summer), Sep-Nov (autumn), Dec-Feb (winter).
 - Southern: Sep-Nov (spring), Dec-Feb (summer), Mar-May (autumn), Jun-Aug (winter).
- **Sun azimuth** (sunlight direction, clockwise from north):
 - 0°: north.

```

    • 45°: northeast.
    • 90°: east.
    • 135°: southeast.
    • 180°: south.
    • 225°: southwest.
    • 270°: west.
    • 315°: northwest.
  - Sun elevation (above horizon):
    • Low (~0°): long shadows.
    • Medium (~45°): moderate shadows.
    • High (~90°): minimal shadows.

</metadata-interpretation-guide>
<objective>
Analyze the two satellite images to describe both changes and unchanged aspects
between them. Provide a comprehensive analysis that covers visual differences
and similarities across all observable elements, including but not limited to key
objects, land cover, structures, vegetation, water bodies, urban development,
natural features, and any other relevant aspects. Use the provided geospatial
metadata only as a reference to inform your analysis, not make it the main
focus or describe it directly. Instead, convert relevant metadata into natural,
descriptive language without including raw numerical values or technical terms
like degrees, percentages, or coordinates. Explain visual influences on changes
and unchanged aspects, ensuring descriptions are reasonable, accurate, and not
dominated by metadata details or speculation.
</objective>
<response-format>
Output as a structured JSON object:
{
  "temporal_caption": "A comprehensive caption describing both the
    changes and unchanged aspects between the two images.",
  "Post-temporal_image_generation": "A textual prompt for
    generating the Post-temporal image, phrased as 'A satellite
    image showing [detailed predicted changes based on observed
    differences].'"
}
</response-format>

```

Fig. 10: Prompt template for draft generation using Qwen3-VL-32B-Instruct in the scalable data construction pipeline.

Text Refinement Prompt

System Prompt

You are an advanced AI model specialized in refining geospatial analyses, correcting and polishing temporal captions, and enhancing image generation prompts based on satellite imagery insights.

You are provided with geospatial metadata and initial analysis outputs for two satellite images of the same geographic location, centered at coordinates (latitude, longitude) (`{center_lat_lon}`), but captured at different times. Geospatial metadata includes:

- **Acquisition times:** Pre-temporal image at `{time[0]}`, Post-temporal image at `{time[1]}`.
- **Bounding boxes for key objects** (normalized coordinates in the range [0, 1000]): Pre-temporal image `{"bbox_2d": {new_xyxy_box[0]}, "label": "{category[0]}"`, Post-temporal image `{"bbox_2d": {new_xyxy_box[1]}, "label": "{category[1]}"`.
- **Sun azimuth:** Pre-temporal image `{sun_azimuth[0]}` degrees, Post-temporal image `{sun_azimuth[1]}` degrees.
- **Sun elevation:** Pre-temporal image `{sun_elevation[0]}` degrees, Post-temporal image `{sun_elevation[1]}` degrees.
- **Off-nadir angle:** Pre-temporal image `{off_nadir_angle[0]}` degrees, Post-temporal image `{off_nadir_angle[1]}` degrees.
- **Cloud cover:** Pre-temporal image `{cloud_cover[0]}`%, Post-temporal image `{cloud_cover[1]}`%.

The following are the initial outputs from a previous analysis:

- **temporal_caption:** `"{temporal_caption}"`.
- **Post-temporal_image_generation:** `"{post_temporal_image_generation}"`.

<metadata-interpretation-guide>

- **Hemisphere:** Positive latitude = Northern; negative = Southern.
- **Seasons (month-based):**
 - Northern: Mar-May (spring), Jun-Aug (summer), Sep-Nov (autumn), Dec-Feb (winter).
 - Southern: Sep-Nov (spring), Dec-Feb (summer), Mar-May (autumn), Jun-Aug (winter).
- **Sun azimuth** (sunlight direction, clockwise from north):
 - 0°: north.
 - 45°: northeast.
 - 90°: east.
 - 135°: southeast.
 - 180°: south.

- 225°: southwest.
 - 270°: west.
 - 315°: northwest.
- **Sun elevation** (above horizon):
- Low ($\sim 0^\circ$): long shadows.
 - Medium ($\sim 45^\circ$): moderate shadows.
 - High ($\sim 90^\circ$): minimal shadows.

</metadata-interpretation-guide>

<objective>

Refine and polish the provided temporal_caption and Post-temporal_image_generation based on the context and metadata guide.

For the temporal_caption:

- Correct any inaccuracies or inconsistencies with the geospatial metadata.
- Improve clarity, conciseness, and flow for better readability.
- Ensure it comprehensively covers both changes (e.g., urban development, vegetation shifts) and unchanged aspects (e.g., stable land features) across all observable elements.
- Naturally incorporate metadata insights (e.g., lighting effects, seasonal influences) into descriptive language without using raw numerical values or technical terms.

For the Post-temporal_image_generation:

- Reference key details from the refined temporal_caption to supplement important information (e.g., add specific predicted changes, visual effects from metadata).
- Enhance it to be a more detailed, vivid prompt for image generation, focusing on observed differences and alignments with the caption.
- Keep the phrasing as ‘A satellite image showing [detailed predicted changes based on observed differences].’
- Avoid speculation; base enhancements on provided analysis.

Use the provided geospatial metadata only as a reference to inform your analysis, not make it the main focus or describe it directly. Instead, convert relevant metadata into natural, descriptive language without including raw numerical values or technical terms like degrees, percentages, or coordinates.

</objective>

<response-format>

Output as a structured JSON object:

```
{
  "temporal_caption": "Refined comprehensive caption describing
    both the changes and unchanged aspects between the two images
    .",
```

```

    "Post-temporal_image_generation": "Enhanced textual prompt for
    generating the Post-temporal image, phrased as 'A satellite
    image showing [detailed predicted changes based on observed
    differences].'"
  }
</response-format>

```

Fig. 11: Prompt template for text refinement with Qwen2.5-72B-Instruct in the data construction pipeline.

ST-CQA GPT-Score Prompt

Evaluate a model-generated change caption against a human-generated caption (ground truth) for the SAME area in pre-/post-temporal remote sensing images. Identify the aspects mentioned in the human caption (both changes and unchanged aspects) and calculate the percentage of these aspects correctly mentioned or partially matched in the model caption. Score from 0 to 100, where each aspect contributes equally to the score. Consider similar concepts for partial score. Provide your score (0–100) and a short justification (less than 15 words) in the format of ‘score#reason’.

Now score the following:
 Human: {ground_truth}
 Model: {model_output}
 Output:

Fig. 12: Prompt used by GPT-5-Nano to compute GPT-Score for the spatiotemporal change understanding (ST-CQA) task.

RS-WorldModel Stage-1 System Prompt

You are a remote sensing world model. Based on the provided particulars, you can generate future remote sensing imagery at any specified time in the future.

Fig. 13: System prompt for RS-WorldModel in Stage 1 (Geo-Aware Generative Pre-training, GAGP).

RS-WorldModel Stage-2/3 System Prompt

You are a remote sensing world model. Based on the provided particulars, you can understand the images and generate future remote sensing imagery at any specified time in the future.

Fig. 14: System prompt for RS-WorldModel used in Stage 2 (Synergistic Instruction Tuning) and Stage 3 (Verifiable Reinforcement Optimization).

TFSF GPT-Score Prompt

You are a strict judge for remote sensing future-image prediction.
[TEXT_DESCRIPTION]
 {text_description}

[PROMPT_METADATA]
 {meta_tse}

Return TWO integer scores (0–50) and one-sentence reason.
(Similarity_score (0–50): Text-Image Consistency
 Evaluate whether the predicted post image matches **TEXT_DESCRIPTION**.
 Use **PROMPT_METADATA** only to penalize obvious contradictions (e.g., target cloud=0 but heavy clouds). Do not require exact physics.

Quality_score (0–50): Image Quality
 Evaluate the predicted post image as a remote sensing image: whether the scene looks realistic for the Earth surface and whether edges/boundaries are visually reasonable.
 Focus on (1) scene realism/plausibility (no obviously impossible or incoherent land-cover/land-use patterns) and (2) edge/boundary quality (no wobbly/-jagged/double edges, halos, boundary bleeding, or melting).

Output **STRICTLY** one-line JSON:
 {"Similarity_score": <int 0-50>, "Quality_score": <int 0-50>,
 "reason": "<one sentence>"}

Fig. 15: Prompt used by GPT-4o to compute GPT-based scores for the text-guided future scene forecasting (TFSF) task.

LLM-as-a-Judge Prompt

Evaluate the Model caption against the Human caption (ground truth) for the SAME area in pre-/post-temporal remote sensing images.

Compare the key information stated in Human and Model for each dimension (changes, unchanged, time, space, environment). Give full/partial credit for semantically consistent information and reduce for contradictions. Score 0–100 using 5 dimensions (20 points each).

Output EXACTLY one line: **score#reason** (reason is one sentence).

PROMPT_METADATA:
{meta_tse}

Human Caption:
{ground_truth}

Model Caption:
{model_output}

Output:

Fig. 16: LLM-as-a-Judge prompt template based on Qwen3-30B-A3B-Instruct-2507 for verifiable reinforcement optimization (VRO).